Thin Solid Films 666 (2018) 185–190

Contents lists available at ScienceDirect

Thin Solid Films

journal homepage: www.elsevier.com/locate/tsf

Enhanced thermoelectric performance of Ga-doped ZnO film by controlling crystal quality for transparent thermoelectric films

Atsuki Tomeda[a], Takafumi Ishibe[a], Tatsuhiko Taniguchi[a], Ryo Okuhata[a], Kentaro Watanabe[a], Yoshiaki Nakamura[a,b,*]

[a] Osaka University, 1-3 Machikaneyama-cho, Toyonaka, Osaka 560-8531, Japan
[b] CREST, JST, 4-1-8 Honcho Kawaguchi, Saitama 332-0012, Japan

ARTICLE INFO

Keywords:
Thermoelectric materials
Zinc oxide
Sol-gel method
Pulsed laser deposition
Thermal conductivity
Thin films
Grain boundary
Interface

ABSTRACT

ZnO, a wide bandgap (3.3 eV) semiconductor has been expected to be a transparent thermoelectric material for the purpose of energy harvesting application because it is a low-cost and ubiquitous element material with a high optical transmittance and a high power factor. Bulk Ga-doped ZnO (GZO) is expected to have higher electrical conductivity and lower thermal conductivity than bulk Al-doped ZnO. However, because reports on their thermoelectric properties of GZO films have been scarce up to now, it has been unclear what film characters affect the thermoelectric properties effectively. In this work, GZO thin films with different characters (*c*-axis orientation, crystal domains and the domain interfaces, and carrier activation rate) were fabricated by two different methods, sol-gel method and pulsed laser deposition. All samples have optical transmittance over 80% in visible range. The highly-oriented GZO films exhibit the highest power factors up to 2.8 $\mu Wcm^{-1}K^{-2}$ in the reported GZO materials and low thermal conductivities of 8.4 $Wm^{-1}K^{-1}$ (1/4 as high as that of bulk GZO). This enhanced thermoelectric performance is attributed to the high carrier activation rate, and the interfaces of highly-oriented crystal domains with the small carrier scattering effect.

1. Introduction

Thermoelectric materials have attracted much attention as an application for energy harvesting from global waste heat sources, such as stand-alone power sources of sensors for IoT society or supplemental clean energy sources for solving global warming issue. Among many applications of thermoelectric materials, we focused on transparent thermoelectric film devices for opening up an application to the stand-alone energy sources placed on the hot glass windows of the building and cars, and on displays of PC or smart phone. Materials for the above applications have to satisfy the following conditions. First, they must be thermoelectric films with high thermoelectric dimensionless figure of merit ZT ($=S^2\sigma T/\kappa$), where S is a Seebeck coefficient, σ is an electrical conductivity, T is an absolute temperature, and κ is a thermal conductivity. Second, these films must have a high optical transmittance in the visible range for the transparency. Third, the film materials should be non-toxic and cost-effective for global applications.

In this sense, conventional heavy metal thermoelectric materials, such as Bi_2Te_3 and PbTe [1,2], are not suitable for the global energy harvesting applications because they are expensive and toxic. Recently, it was theoretically predicted that the use of nanostructures or film structures could elevate ZT value of materials, where S is enhanced by quantum confinement [3] or energy filtering effect [4] and κ is reduced by phonon scattering effect [5–7]. Therefore, the nanostructure [8–11] or film structure composed of ubiquitous materials with transparent, cost-effective, and non-toxic nature became a potential thermoelectric material for the global energy harvesting applications.

A transparent wide bandgap (~3.3 eV) semiconductor zinc oxide (ZnO), which bulk [12,13] and nanostructures [14–17] have been intensively studied, is a promising material in various application fields: transparent electrode [18], gas sensor [19,20], piezoelectric device [21], and so on. Bulk ZnO materials exhibit a high power factor $S^2\sigma$ (~10–20 $\mu Wcm^{-1}K^{-2}$) [12,22,23] but also high κ [12,22,24]. The high κ bottlenecked their thermoelectric applications. As for the films, J. Loureiro, et al., reported thermoelectric properties of Al-doped ZnO (AZO) films fabricated by the magnetron sputtering where low κ value was reported at 300 K [25]. However, κ reduction sacrifices their $S^2\sigma$ values to some extent [25]. Thus, $S^2\sigma$ enhancement as well as κ reduction of ZnO thin films are required for their transparent thermoelectric applications.

* Corresponding author.
E-mail address: nakamura@ee.ec.osaka-u.ac.jp (Y. Nakamura).

https://doi.org/10.1016/j.tsf.2018.09.045
Received 14 March 2018; Received in revised form 20 August 2018; Accepted 26 September 2018
Available online 27 September 2018
0040-6090/

We focus on the Ga-doped ZnO (GZO) films instead of AZO films for the following reasons. In terms of electron transport, GZO is expected to realize a higher electron mobility than AZO because a substitutional Ga at Zn site in GZO induces smaller local lattice deformation than that in the AZO case due to the bond length of Ga−O (0.192 nm) closer to Zn−O (0.197 nm) than that of Al−O (0.181 nm). [26] As for the phonon transport, GZO is expected to have lower than AZO due to the effective phonon scattering at heavy Ga ions. [12] Moreover, GZO has an application advantage: higher resistivity to oxidation degrading the electrical conductivity than AZO [27], and lower stress-strain constraints on doping, and so on. [28] Unlike AZO films, however, the reports on the thermoelectric properties of GZO films are scarce up to now [29,30]. A report about non-oriented sol-gel GZO films grown by isopropyl alcohol (IPA) solution process [29] exhibited low thermoelectric power factor, $S^2\sigma$ (1.9 μWcm^{-1}K^{-2}) due to poor electron mobility in low crystal quality films. This implies a possibility that enhancement of film crystal quality increases the electron mobility resulting in large $S^2\sigma$. Thus, the systematic investigation of the relation between film crystal quality and thermoelectric performance is important, but there have been no reports about impacts of film characters on thermoelectric properties in GZO films: crystal orientations, crystal domain sizes and the interfaces. Unlike *non-oriented* sol-gel films [29,30], *oriented* GZO films by pulsed laser deposition (PLD) and sol gel processes have not been studied for its thermoelectric application although films have better controllability of crystal domain orientation than bulk GZO [31].

In this work, we thoroughly investigate the thermoelectric properties depending on the structural characters of GZO films. To control the orientation, size and interfaces of crystal domains, oriented sol-gel films synthesized by 2-methoxyethanol solution process [31] and highly-oriented PLD films were fabricated. The crystal orientation of GZO films would rather be a key for the thermoelectric performance than the interface density and the domain size. As a result, highly-oriented GZO films exhibited the highest $S^2\sigma$ of ~2.8 μWcm^{-1}K^{-2} in the reported GZO materials although the carrier concentration is not optimized yet. The thermal conductivity at the out-of-plane direction exhibited ~1/4 reduction (~8.4 Wm^{-1}K^{-1}) compared with bulk GZO (κ~29 Wm^{-1}K^{-1}) [32], demonstrating that the highly-oriented films is a promising for thermoelectric film devices.

2. Experimental methods

To investigate the impact of the film characters, we fabricated the films with various qualities as follows. As moderate quality films, (0001)-oriented polycrystalline GZO films were synthesized by sol-gel process, while as high quality films, highly-oriented polycrystalline GZO films were fabricated by PLD process.

For PLD of GZO thin films, GZO targets with nominal Ga content of 0.1–2.0 at% were fabricated by sintering process; mixed powder of ZnO (99.999% purity) and Ga_2O_3 (99.99% purity) was pressed at the pressure of 8 MPa followed by being sintered at 1100 °C for 24 h. The above GZO targets, the quartz glass (5 × 10 × 0.5 mm^3), and the undoped Si (111) substrates (5 × 10 × 0.3 mm^3) were introduced into PLD vacuum chamber at a base pressure of ~1 × 10^{-6} Pa. The GZO targets were put 40 mm away from the substrates (quartz glass and Si). The GZO films were grown on these substrates for 2 h at the temperature of 325 °C in oxygen partial pressure of 0.2 Pa (as-grown sample), where ArF excimer laser (wavelength of 193 nm, pulse energy of 60 mJ, and pulse repetition rate at 10 Hz) was used for laser ablation of the above GZO targets. Some of as-grown GZO film samples were annealed at 400 °C in vacuum of 10^{-5} Pa for 10 min to enhance the film crystallinity (annealed sample).

For sol-gel synthesis of GZO films with better alignment of crystal domain orientations than those reported [25,28], precursor solution was prepared by dissolving monoethanolamine (0.5 M), zinc acetate dehydrate ($Zn(CH_3CO_2)_2{\cdot}2H_2O$, 0.5 M), and gallium chloride ($GaCl_3$) in 2-methoxyethanol at 60 °C for 2 h. Ga molar ratio, [Ga]/([Ga] + [Zn]) in the solution, which is nominal Ga content in the case of sol-gel synthesis, was varied in the range of 0.5–2.0 at%. The quartz glass (10 × 10 × 0.5 mm^3) and the undoped Si(111) substrates (10 × 10 × 0.3 mm^3) were cleaned ultrasonically in ethanol, acetone, and deionized water. These cleaned substrates were spin-coated with the above precursor solution at the speed of 3000 rpm for 30 s. The spin-coated films were dried in 350 °C for 10 min in the air as preheat treatment. This film coating process and preheat treatment were repeated 4 times. Finally, for the crystal growth, these spin-coated films were postheated at 700 °C for 1 h under the N_2 gas flow (1 L/min) at atmospheric pressure, resulting in the formation of GZO films (as-grown sample). Some of as-grown GZO film samples were annealed at 530 °C in vacuum of 10^{-5} Pa for 2 h (annealed sample) to enhance the film crystallinity.

The surface morphologies of the GZO films were observed by atomic force microscope (AFM). The crystallinity of the GZO films was investigated by x-ray diffraction (XRD) using Cu K_α line (1.5406 Å in wavelength). The transmittance of the samples was measured in the wavelength range of 190–900 nm by ultraviolet-visible (UV–Vis) spectroscopy. The GZO film thickness and domain sizes were observed by scanning electron microscope (SEM), where typical thicknesses of PLD GZO films and sol-gel GZO films were around 200 nm and around 100 nm, respectively. Hall effect measurement of the GZO films/quartz glass was performed to evaluate σ and electron mobility μ. S was also measured by conventional apparatus (ZEM-3, Advance Riko Inc.). κ of the GZO film/Si substrates was measured at the out-of-plane direction by 2ω method (Advance Riko Inc.), where Cr films (~160 nm in thickness) deposited on the GZO film surfaces were used both as Joule heaters for the surface temperature modulation and as standard materials for the thermoreflectance (TR) measurement. [33] All thermoelectric properties were measured at room temperature (RT). In this work, films were formed on two kinds of substrates, quartz glass and Si. For the thermal conductivity measurements, the films on undoped Si substrates were used, while films on insulator quartz glasses were investigated for other measurements in order to get rid of the contribution of carrier transport in substrates.

3. Results and discussion

Fig. 1 shows XRD results of the sol-gel and PLD GZO films on quartz glass substrates with nominal Ga content of 2.0 at%, respectively. In addition to as-grown films, vacuum-annealed samples are also displayed. There are almost no differences between as-grown and annealed samples in XRD results, indicating there are no changes of crystallographic characters after annealing in vacuum. In XRD 2θ-ω scan (Fig. 1(a)), all GZO films exhibited 0002_{ZnO} and 0004_{ZnO} diffraction peaks at around 34° and 72°, respectively. This indicates that

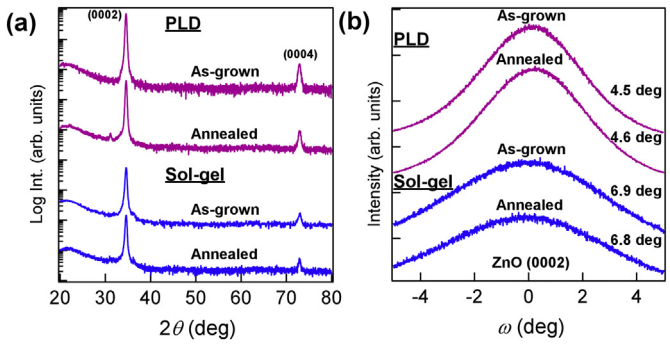

Fig. 1. XRD results of the sol-gel and PLD GZO films on quartz glass substrates with nominal Ga content of 2.0 at%. In addition to as-grown films, vacuum-annealed samples are also displayed. 2θ-ω scans (a) and ω scans around $(0002)_{ZnO}$ diffraction spot with the FWHMs of the peaks (b).

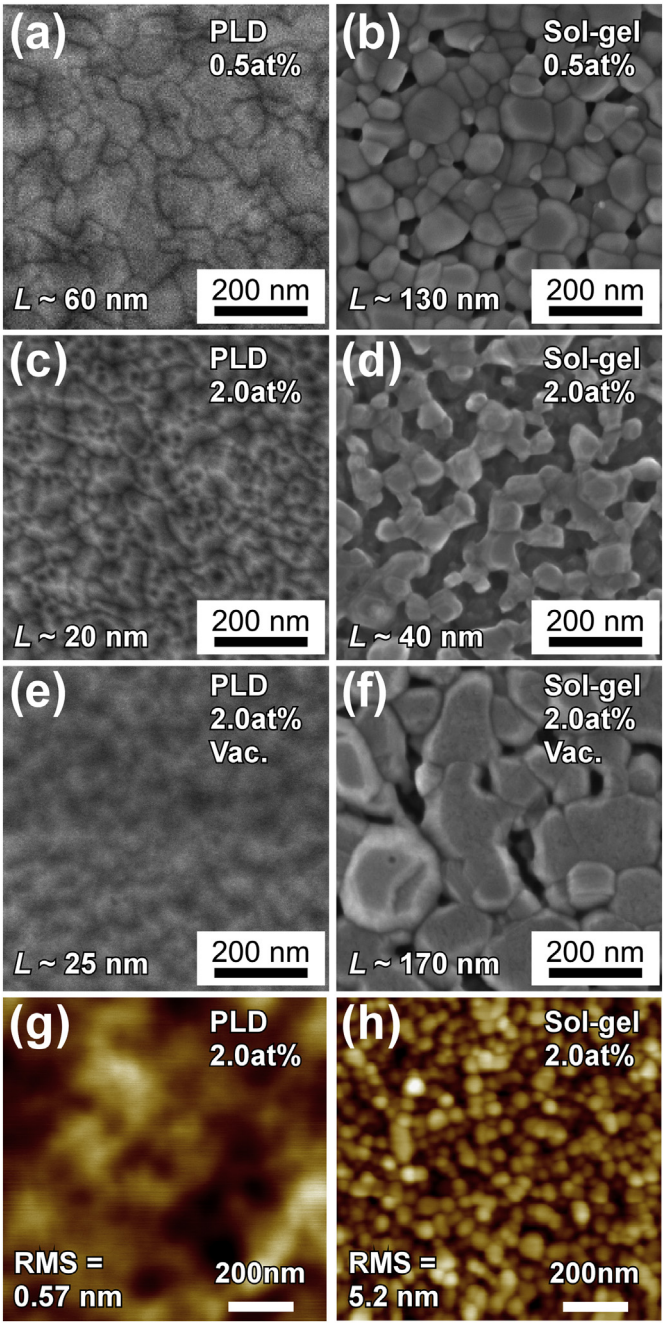

Fig. 2. (a)–(d) SEM images of as-grown GZO films with nominal Ga content of 0.5 at% and 2.0 at% which were grown by PLD or by sol-gel method. (e)–(f) SEM images of annealed PLD and sol-gel GZO films with nominal Ga content of 2.0 at%. (g)–(h) AFM images of as-grown PLD and sol-gel GZO films with nominal Ga content of 2.0 at%.

unlike the previous report of non-oriented sol-gel GZO films synthesized by IPA solution process [29], our sol-gel films synthesized by 2-methoxyethanol solution process were successfully oriented. Fig. 1(b) displays XRD ω scans (rocking curves) around 0002_{ZnO} diffraction spot with full-width-at-half-maximums (FWHM) of their peaks. PLD and sol-gel GZO films exhibited sharp (FWHM of 4.5°-4.6°) and broad peaks (FWHM of 6.8°-6.9°), respectively. Although these results indicated that PLD and sol-gel GZO films were both oriented to $(0001)_{ZnO}$, there are some differences between them in terms of either the degree of orientation or domain size; PLD films have either highly-oriented domains or large domains compared with sol-gel films.

Figs. 2(a)–(f) show SEM images of PLD and sol-gel GZO films with nominal Ga content of 0.5 and 2.0 at%. Average size of GZO crystal domain, L is also denoted in each panel. AFM images in Figs. 2(g) and (h) show surface morphologies of PLD and sol-gel GZO films with nominal Ga content of 2.0 at%. Root mean square (RMS) value of the surface morphology is denoted in each panel. These results demonstrated that PLD GZO films have flatter surface structures with smaller domains compared with sol-gel GZO films (rougher surfaces and larger domains). By considering the results about the sharper peaks in XRD rocking curves in PLD GZO films, it is proved that the PLD GZO films were composed of relatively-small, but highly-(0001) oriented domains with a high areal density, whereas sol-gel GZO films consisted of larger domains with less degree of the orientation. Because crystal domain orientation, domain size, and domain interface density strongly affect the carrier transports in general, the two kinds of the films with such different characters are useful to clarify which film characters (crystal orientation, crystal domain size and domain interface character) affect the thermoelectric properties effectively.

There are two common remarkable facts in both PLD and sol-gel films: domain size decreased (domain interface density increased) with increase of nominal Ga content GZO films, and vacuum-annealing process increased domain size. Ga content dependence implies that Ga atoms can supply nucleation sites resulting in the large number of domains with smaller size (increase of the interface density).

The optical transmittance spectra of as-grown GZO films with different nominal Ga content up to 2.0 at% were measured in Figs. 3(a) and (b).

It was confirmed that all samples had high optical transmittance over 80% in visible range. The PLD GZO films exhibited oscillation in the transmittance spectra due to the optical interference between the flat film surfaces and the interfaces. The differences in peak wavelengths of the interference among spectra originated from the differences of film thicknesses (160–300 nm). Tauc plots $[(\alpha h\nu)^2$ vs $h\nu]$ of as-grown PLD and sol-gel GZO films were obtained from their optical transmittance spectra as shown in Figs. 3(c) and (d), respectively, where α is an optical absorption coefficient, h is Planck coefficient, ν is photon frequency. Optical bandgap E_g^{opt}, corresponding to the x-intercept in Tauc plot, increases with increase of nominal Ga content. Fig. 3(e) shows E_g^{opt} as a function of electron concentration n obtained from Hall effect measurement result. Both as-grown PLD and sol-gel GZO films exhibited a monotonic increase of E_g^{opt} with n. This blue shift of E_g^{opt} at higher n (higher Ga content) is accountable by Burstein-Moss effect [34], which is described by the following equation,

$$E_g^{opt} = E_g(0) + \Delta E_g^{BM} = E_g(0) + \frac{h^2}{8m^*}\left(\frac{3}{\pi}\right)^{2/3} n^{2/3} \quad (1)$$

where E_g (0) is energy bandgap of undoped ZnO crystal, ΔE_g^{BM} is the shift energy by Burstein-Moss effect and m^* is electron effective mass in conduction band. The data in Fig. 3(e) is fitted with Eq. (1) as shown in the solid line when m^* is adjusted to be 0.3 times free electron mass m_0.

The relation between electron Hall concentration n and nominal Ga content is displayed in Fig. 4(a) with reference lines of carrier activation rates (0.01, 0.1 and 1), indicating the higher carrier activation rate in PLD GZO films compared with sol-gel GZO films. This higher n in PLD GZO films due to its higher carrier activation rate is consistent with larger optical bandgap in PLD GZO films by Burstein-Moss effect than sol-gel GZO films as shown in Fig. 3(e).

Figs. 4(b)–(e) show thermoelectric properties of our GZO films with different nominal Ga content (solid (open) circles and squares for as-grown (annealed) PLD and sol-gel films, respectively). The data of sol-gel GZO films, sputtered AZO films, and bulk ones that are reported by other groups [24,29,30,32] are also plotted for reference (triangles, pentagons, crosses, and diamonds). Figs. 4(b) and (c) show σ and μ of GZO films at different n. Solid lines are semi-empirical curves fitted to the experimental plots for single-crystalline ZnO [35]. Our oriented sol-gel GZO films (squares) exhibited higher σ and μ at the lower n region

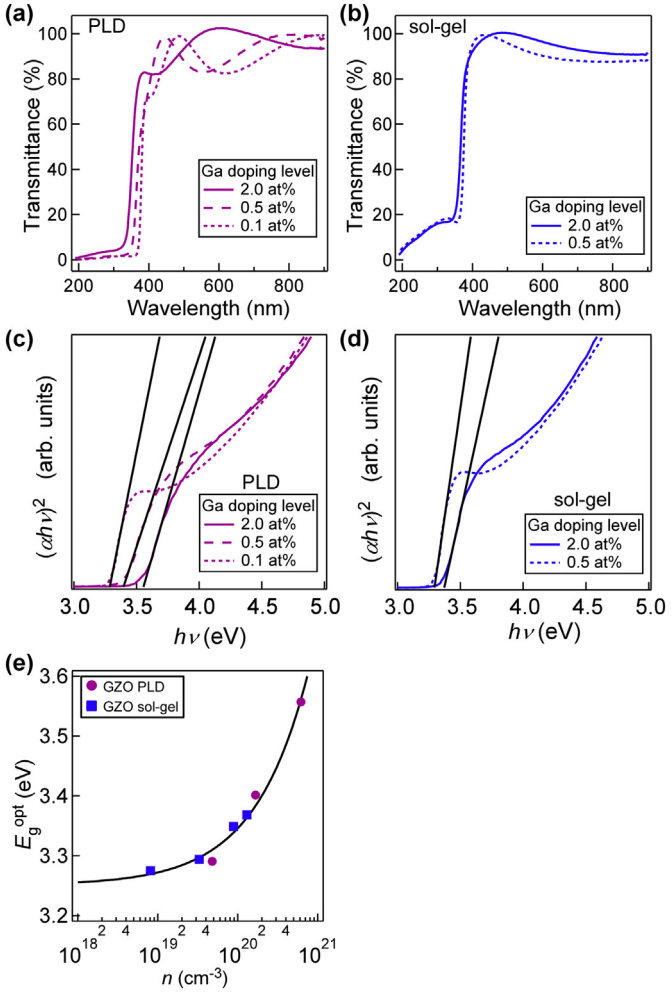

Fig. 3. (a)–(b) optical transmittance spectra of as-grown GZO films with different nominal Ga content up to 2.0 at%, formed by PLD (a) and sol-gel method (b), respectively. (c)–(d) Tauc plot [$(\alpha h\nu)^2$ vs $h\nu$] of as-grown PLD (c) and sol-gel GZO films (d), respectively, obtained from their optical transmittance spectra. (e) Optical bandgap of as-grown GZO films at difference carrier concentration. Line is a fitted curve with Eq. (1).

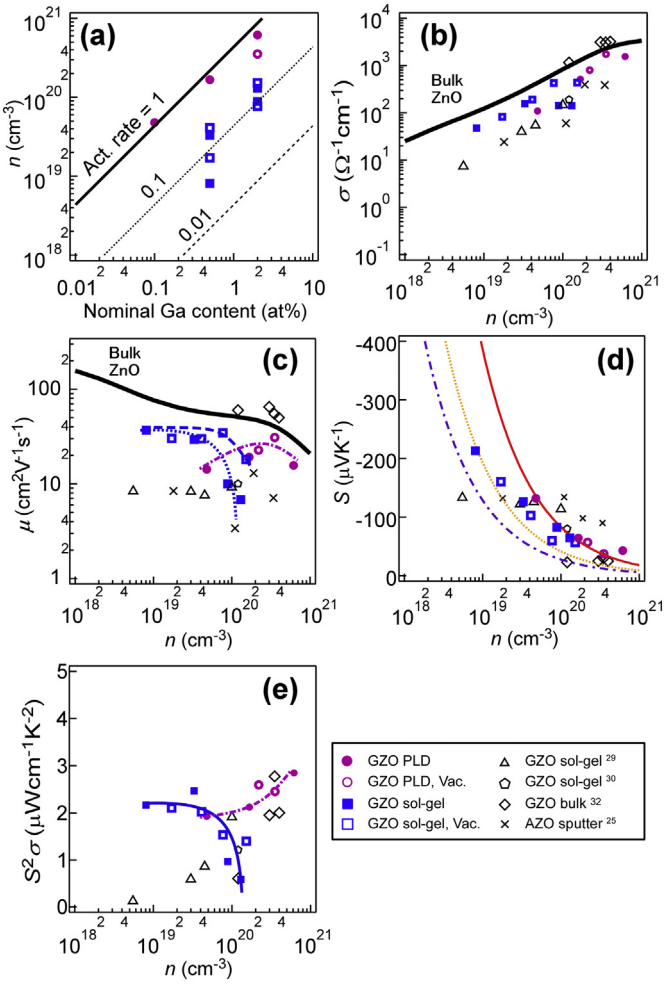

Fig. 4. (a) Electron Hall concentration of GZO films plotted against nominal Ga content with reference lines describing carrier activation rates of 0.01, 0.1, and 1. (b)–(e) σ, μ, S, and $S^2\sigma$ of GZO films at different n. Lines in (d) are calculated S values based on Eq. (2) with scattering parameter, y of −0.5 (the dashed one), 0 (the dotted one), and 1.5 (the solid one).

($< 5 \times 10^{19}\,\mathrm{cm}^{-3}$) compared with the non-oriented sol-gel films via IPA solution process reported by other groups' (triangles) [29]. By considering that our sol-gel films are oriented, and that previously-reported films are non-oriented, this is a strong evidence of the large influence of the crystal orientation on the σ and μ at lower n region. However, at higher n regions, μ are dropped with increase of n (dotted and dashed lines). Such a drop of μ was reported to be caused by domain interface scattering [36]. Furthermore, by considering that this drop is smaller in annealed sol-gel films with larger domain size (small domain interface density) than as-grown films with smaller domain size (large domain interface density) as shown in Fig. 4(c), it was found that at the higher n regions, in addition to the charged donor scattering, electron scattering at domain interfaces also occurred, which strongly depended on the domain interface characters, resulting in the reduction of the μ. It is an open question of appearance of domain interface scattering effect at the high n region in the sol-gel film case.

In contrast, PLD GZO films exhibited high σ (high μ) at high $n > 2 \times 10^{20}\,\mathrm{cm}^{-3}$ (chain line), despite the low σ and μ at the low n. This is easy to understand by considering as follows: at lower n, electron scattering at the domain interfaces are dominant because of its domains with small size and high density. However, with increase of n, electron scattering by charged donors becomes dominated. At the high n, carrier transport is the same mechanism as that of the bulk with high μ shown by the solid line at high n in Fig. 4(c). In this framework, it is assumed that the contribution of domain interface scattering is negligible due to the dominant charged donor scattering at high n. This does not always work out. As mentioned above, in sol-gel films, interface scattering appeared at high n in addition to charged donor scattering. On the other hand, the lack of interface scattering in the PLD films is responsible for good interface character due to the high orientation of the domains forming the interfaces. Therefore, this bulk-like high μ is attributed both to the high carrier activation rate of substitutional Ga and to the better interface due to the high crystal orientation.

Fig. 4(d) shows S of the GZO films. For reference, $S(n)$ lines of ZnO films due to specific carrier scattering mechanisms were theoretically calculated with Eq.(2) as shown by solid, dotted and dashed lines in Fig. 4(d). The Eq. (2) is described as.

$$S = \frac{8\pi^2}{3}\left(\frac{\pi}{3}\right)^{\frac{2}{3}}\left(y + \frac{3}{2}\right)\frac{k^2 m^* T}{eh^2 n^{\frac{2}{3}}} \tag{2}$$

where k is Boltzmann constant, e is electron charge, and y is a scattering parameter [35]. Here, m^* is found to be $0.3m_0$ from Burstein-Moss effect. As for y, $y = 1.5$ describes carrier scattering that is dominantly caused by ionized impurities such as charged donors (solid line). On the other hand, the dotted and dashed lines are calculated ones of Eq. (2) with $y = 0$ and -0.5, respectively, where carriers are considered to be scattered by neutral impurities or nonionized defects

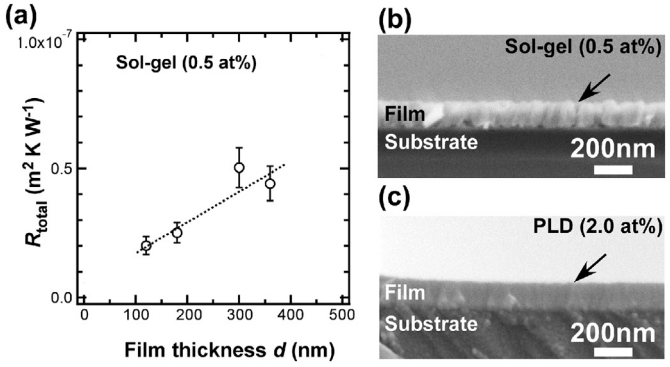

Fig. 5. (a) Thicknesse dependence of the thermal resistance, R_{total} of 0.5 at% sol-gel GZO films measured by 2ω method. The sum of interfacial thermal resistances at Cr/GZO and GZO/Si, R_{int} and a thermal conductivity of GZO film, κ were evaluated by fitting with $R_{total} = R_{int} + d/\kappa$ with weighted with their errors ($R_{int} = 5.3 \pm 5.7 \times 10^{-9}$ m^{2}KW^{-1}, $\kappa = 8.4 \pm 2.0$ Wm^{-1}K^{-1}). Cross-sectional SEM images of (b) sol-gel GZO (0.5 at%) and (c) PLD GZO (2.0 at%). Both GZO films are (0001)ZnO-oriented polycrystals with crystal domains extending in out-of-plane directions. One of the domain boundaries is indicated by solid arrow in each panel.

dominantly. [35,37] Fig. 4(d) indicates that all PLD GZO films are governed by charged donor scattering in their entire range. This is due to high Ga carrier activation rates of the order of unity as shown in Fig. 4(a). In contrast, at low $n = 8 \times 10^{18}$ cm^{-3}, sol-gel GZO films exhibited small S due to carrier scattering effect by neutral impurity (nonionized defects) compared with solid line (charged donor scattering). The films are gradually dominated by charged donor scattering with increasing n up to high value of 1×10^{20} cm^{-3}. The neutral impurity (nonionized defects) effect at low n comes from the low activation rates of sol-gel GZO films.

A $S^2\sigma$ of GZO films with respect to their n is shown in Fig. 4(e), where previously reported data of GZO materials including the same impurities (Ga) are shown to reveal electron transport in films with various crystal domains in the same material system. Evidently, highly-oriented PLD GZO films exhibited the highest $S^2\sigma$ (2.8 μWcm^{-1}K^{-2}) in the reported GZO materials (GZO bulks [32] and GZO films [29,30]). In addition, our oriented sol-gel GZO films, which have the lower extent of orientation than our PLD GZO films, exhibited higher $S^2\sigma$ than non-oriented sol-gel GZO films reported previously. This suggested that the domain alignment in (0001)-orientation is a key to suppress electron scattering at crystal domain interfaces to enhance $S^2\sigma$.

Out-of-plane thermal conductivities κ of GZO film/Si substrates with various film thicknesses, d were measured by 2ω method, where Cr films were formed on the film surfaces. The measured thermal resistances R_{total} of 0.5 at% sol-gel GZO films were shown in Fig. 5. The R_{total} values include a sum of thermal interfacial resistances R_{int} at two interfaces of Cr/GZO and GZO/Si, and then we fitted R_{total} values with $R_{total} = R_{int} + d/\kappa$ weighted by their experimental errors (the broken line) assuming negligible dependence of κ on d. This assumption may not work in high quality films where there are phonons with longer mean free paths (MFPs) than film thickness. This brings strong d dependence of κ [38]. In the present sol-gel GZO films with poor crystallinity, we were able to consider the small phonon MFP and the resultant weak d dependence. Then, the values of κ and R_{int} were acquired to be 8.4 ± 2.0 Wm^{-1}K^{-1} and 5.3 ± 5.7 × 10^{-9} m^{2}KW^{-1} from the slope and offset of the fitting line, respectively. The obtained R_{int} value was roughly accountable by a sum of theoretical interfacial thermal resistances of Cr/ZnO (1.4×10^{-9} m^{2}KW^{-1} [39]) and ZnO/Si (1.9×10^{-9} m^{2}KW^{-1} [39]) although the deviation of R_{int} coming from fitting error is large. The obtained κ is similar to the reported thermal conductivity 4–7 Wm^{-1}K^{-1} of sputtered AZO films with 5% Al content [40]. This low κ is 1/4 times as large as the bulk GZO (1.5 at%, $\kappa = 29$ Wm^{-1}K^{-1} [32]). It should be noted that this κ value is the one of formed ZnO material itself without the film structure effect: namely phonon surface scattering effect and phonon interface scattering effect between substrate and film because this κ value was obtained without R_{int} from the slope of thickness dependence, not from one sample measurement. Therefore, it is considered that this small κ value could be attributed to the phonon scattering at the crystal domain interfaces inside the polycrystalline GZO films.

Here, we discuss the thermoelectric performance of (0001)-oriented PLD and sol-gel GZO films by considering the measurement direction difference: *in-plane* σ and *out-of-plane* κ. The ZT value at RT was tentatively estimated to be 0.01 (ZT_{low}) using in-plane σ and out-of-plane κ for reference although the ZT_{low} value can be different from the real ZT value measured at the same direction. The in-plane σ and out-of-plane κ can be used to obtain the guideline for ZT enhancement of GZO materials for the following reason. The *out-of-plane* σ in GZO films is expected to be larger than experimental *in-plane* σ, indicating that the ZT_{low} can be a lower limit of ZT. This is justified as follows. Electron moving at the *in-plane* direction runs across crystal domain interface, while electron can transport at the *out-of-plane* direction with almost no interface scattering because both PLD and sol-gel GZO films were (0001)-oriented and have domains elongated along [0001] direction, as shown in Figs. 5(b) and (c). In a similar fashion, in-plane κ is expected to be lower than that at out-of-plane direction, indicating ZT_{low} can be a lower limit of ZT at both directions.

4. Conclusions

To investigate film characters on thermoelectric properties of polycrystalline GZO, we formed two types of GZO films by sol-gel method using 2-methoxyethanol solution and the PLD method, both of which were (0001)-oriented, unlike reported non-oriented sol-gel GZO films using IPA solution. The GZO films had greatly different film characters depending on the fabricating technique. The PLD GZO films had higher crystal orientation, higher carrier activation rate, but smaller domain size (large domain interface density) compared with the sol-gel GZO films using 2-methoxyethanol solution. The PLD GZO films exhibited high S and μ in high n range ($> 10^{19}$ cm^{-3}) because charged donor scattering dominates over domain interface scattering. This is achieved both by the high activation rate (high n) and by the better domain interface with negligible carrier scattering due to the highly-oriented domains. Therefore, highly-oriented PLD GZO films exhibited the highest $S^2\sigma$ (2.8 μWcm^{-1}K^{-2}) in the reported GZO materials. In addition, highly-oriented GZO films have low thermal conductivities ($\kappa = 8.4$ Wm^{-1}K^{-1}) significantly lower than bulk GZO. These results demonstrated that the highly-oriented GZO film with controlled crystal domain and domain interface is a promising transparent thermoelectric material.

Acknowledgments

This work was supported in part by the JST CREST Program. A part of this work was also supported by a Grant-in-Aid for Scientific Research A (Grant No. 16H02078), a Grant-in-Aid for Exploratory Research (Grant No. 15K13276), and the JSPS Research fellow (17J00328). A part of PLD in this work was supported by "Nanotechnology Platform Project (Nanotechnology Open Facilities in Osaka University)" of Ministry of Education, Culture, Sports, Science and Technology, Japan [No. S-17-OS-0025].

References

[1] H.J. Goldsmid, The Electrical conductivity and thermoelectric power of bismuth telluride, Proc. Phys. Soc. 71 (1958) 633–646.
[2] J.P. Heremans, V. Jovovic, E.S. Toberer, A. Saramat, K. Kurosaki, A. Charoenphakdee, S. Yamanaka, G.J. Snyder, Enhancement of thermoelectric

efficiency in PbTe by distortion of the electronic density of states, Science 321 (2008) 554–557.
[3] L.D. Hicks, M.S. Dresselhaus, Effect of quantum-well structures on the thermoelectric figure of merit, Phys. Rev. B 47 (1993) 16631–16634.
[4] D. Vashaee, A. Shakouri, Improved thermoelectric power factor in metal-based superlattices, Phys. Rev. Lett. 92 (2004) 106103.
[5] Y. Nakamura, M. Isogawa, T. Ueda, S. Yamasaka, H. Matsui, J. Kikkawa, S. Ikeuchi, T. Oyake, T. Hori, J. Shiomi, A. Sakai, Anomalous reduction of thermal conductivity in coherent nanocrystal architecture for silicon thermoelectric material, Nano Energy 12 (2015) 845–851.
[6] S. Yamasaka, Y. Nakamura, T. Ueda, S. Takeuchi, A. Sakai, Phonon transport control by nanoarchitecture including epitaxial Ge nanodots for Si-based thermoelectric materials, Sci. Rep. 5 (2015) 14490.
[7] G. Joshi, H. Lee, Y. Lan, X. Wang, G. Zhu, D. Wang, R.W. Gould, D.C. Cuff, M.Y. Tang, M.S. Dresselhaus, G. Chen, Z. Ren, Enhanced thermoelectric figure-of-merit in nanostructured p-type silicon germanium bulk alloys, Nano Lett. 8 (2008) 4670–4674.
[8] Y. Nakamura, K. Watanabe, Y. Fukuzawa, M. Ichikawa, Observation of the quantum-confinement effect in individual Ge nanocrystals on oxidized Si substrates using scanning tunneling spectroscopy, Appl. Phys. Lett. 87 (2005) 133119.
[9] S. Yamasaka, K. Watanabe, S. Sakane, S. Takeuchi, A. Sakai, K. Sawano, Y. Nakamura, Independent control of electrical and heat conduction by nanostructure designing for Si-based thermoelectric materials, Sci. Rep. 6 (2016) 22838.
[10] N. Naruse, Y. Mera, Y. Nakamura, M. Ichikawa, K. Maeda, Fourier-transform photoabsorption spectroscopy of quantum-confinement effects in individual GeSn nanodots, Appl. Phys. Lett. 94 (2009) 093104.
[11] Y. Nakamura, Nanostructure design for drastic reduction of thermal conductivity while preserving high electrical conductivity, Sci. Technol. Adv. Mater. 19 (2018) 31.
[12] M. Ohtaki, K. Araki, K. Yamamoto, High thermoelectric performance of dually doped ZnO ceramics, J. Electron. Mater. 38 (2009) 1234–1238.
[13] D.C. Look, D.C. Reynolds, J.R. Sizelove, R.L. Jones, C.W. Litton, G. Cantwell, W.C. Harsch, Electrical properties of bulk ZnO, Solid State Commun. 105 (1998) 399–401.
[14] K. Watanabe, T. Nagata, S. Oh, Y. Wakayama, T. Sekiguchi, J. Volk, Y. Nakamura, Arbitrary cross-section SEM-cathodoluminescence imaging of growth sectors and local carrier concentrations within micro-sampled semiconductor nanorods, Nat. Commun. 7 (2016) 10609.
[15] K. Watanabe, T. Nagata, Y. Wakayama, T. Sekiguchi, R. Erdélyi, J. Volk, Band-gap deformation potential and elasticity limit of semiconductor free-standing nanorods characterized in situ by scanning electron microscope-cathodoluminescence nanospectroscopy, ACS Nano 9 (2015) 2989–3001.
[16] T. Ishibe, A. Tomeda, K. Watanabe, J. Kikkawa, T. Fujita, Y. Nakamura, Embedded-ZnO nanowire structure for high-performance transparent thermoelectric materials, J. Electron. Mater. 46 (2017) 3020–3024.
[17] Z.R. Tian, J.A. Voigt, J. Liu, B. McKenzie, M.J. McDermott, M.A. Rodrigez, H. Konishi, H. Xu, Complex and oriented ZnO nanostructures, Nat. Mater. 2 (2003) 821–826.
[18] X. Jiang, F.L. Wong, M.K. Fung, S.T. Lee, Aluminum-doped Zinc oxide films as transparent conductive electrode for organic light-emitting devices, Appl. Phys. Lett. 83 (2003) 1875.
[19] J.F. Chang, H.H. Kuo, I.C. Leu, M.H. Hon, The effects of thickness and operation temperature on ZnO:Al thin film CO gas sensor, Sensors Actuators B Chem. 84 (2002) 258.
[20] J. Xu, Q. Pan, Y. Shun, Z. Tian, Grain size control and gas sensing properties of ZnO gas sensor, Sensors Actuators B Chem. 66 (2000) 277.
[21] M. Laurenti, D. Perrone, A. Verna, C.F. Pirri, A. Chiolerio, Development of a flexible Lead-free piezoelectric transducer for health monitoring in the space environment, Micromachines 6 (2015) 1729.
[22] K.P. Ong, D.J. Singh, P. Wu, Analysis of the thermoelectric properties of n-type ZnO, Phys. Rev. B 83 (2011) 115110.
[23] M. Ohtaki, T. Tsubota, K. Eguchi, H. Arai, High-temperature thermoelectric properties of $(Zn_{1-x}Al_x)O$, J. Appl. Phys. 79 (1996) 1816–1818.
[24] K.F. Cai, E. Muller, C. Drasar, A. Mrotzek, Preparation and thermoelectric properties of Al-doped ZnO ceramics, Mater. Sci. Eng. B 104 (2003) 45–48.
[25] J. Loureiro, N. Neves, R. Barros, T. Mateus, R. Santos, S. Filonovich, S. Reparaz, C. Torres, F. Wyczisk, L. Divay, R. Martinsa, I. Ferreira, Transparent aluminium zinc oxide thin films with enhanced thermoelectric properties, J. Mater. Chem. A 2 (2014) 6649–6655.
[26] H.J. Ko, Y.F. Chen, S.K. Hong, H. Wenisch, T. Yao, D.C. Look, Ga-doped ZnO films grown on GaN templates by plasma-assisted molecular-beam epitaxy, Appl. Phys. Lett. 77 (2000) 3761–3763.
[27] J. Nomoto, M. Konagai, K. Okada, T. Ito, T. Miyata, T. Minami, Comparative Study of resistivity characteristics between transparent conducting AZO and GZO thin films for use at high temperatures, Thin Solid Films 518 (2010) 2937–2940.
[28] A. Abduev, A. Akmedov, A. Asvarov, A. Chiolerio, A revised growth model for transparent conducting Ga doped ZnO films: improving crystallinity by means of buffer layers, Plasma Process. Polym. 12 (2015) 725.
[29] G.K. Paul, S.K. Sen, Sol–Gel preparation, characterization and studies on electrical and thermoelectrical properties of gallium doped zinc oxide films, Mater. Lett. 57 (2002) 742–746.
[30] A.Z. Barasheed, S.R.S. Kumar, H.N. Alshareef, Temperature dependent thermoelectric properties of chemically derived gallium zinc oxide thin films, J. Mater. Chem. C 1 (2013) 4122–4127.
[31] M. Ohyama, H. Kozuka, T. Yoko, S. Sakka, Preparation of ZnO films with preferential orientation by Sol-gel method, J. Ceram. Soc. Jpn. 104 (1996) 296–300.
[32] K.H. Jung, K.H. Lee, W.S. Seo, S.M. Choi, An enhancement of a thermoelectric power factor in a Ga-doped ZnO system: a chemical compression by enlarged Ga solubility, Appl. Phys. Lett. 100 (2012) 253902.
[33] R. Okuhata, K. Watanabe, S. Ikeuchi, A. Ishida, Y. Nakamura, Thermal conductivity measurement of thermoelectric thin films by a versatility-enhanced 2ω method, J. Electron. Mater. 46 (2017) 3089–3096.
[34] K.H. Kim, K.C. Park, D.Y. Ma, Structural, electrical and optical properties of aluminum doped zinc oxide films prepared by radio frequency magnetron sputtering, J. Appl. Phys. 81 (1997) 7764–7772.
[35] K. Ellmer, Resistivity of polycrystalline zinc oxide films: current status and physical limit, J. Phys. D 34 (2001) 3097–3108.
[36] John Y.W. Seto, The electrical properties of polycrystalline silicon films, J. Appl. Phys. 46 (1975) 5247–5254.
[37] J.H. Bahk, A. Shakouri, Minority carrier blocking to enhance the thermoelectric figure of merit in narrow-band-gap semiconductors, Phys. Rev. B 93 (2016) 165209.
[38] X. Wu, J. Lee, V. Varshney, J.L. Wohlwend, A.K. Roy, T. Luo, Thermal conductivity of wurtzite zinc-oxide from first-principles lattice dynamics – a comparative study with gallium nitride, Sci. Rep. 6 (2016) 22504.
[39] H. Wang, Y. Xu, M. Shimono, Y. Tanaka, M. Yamazaki, Computation of interfacial thermal resistance by phonon diffuse mismatch model, Mater. Trans. 48 (2007) 2349–2352.
[40] N. Oka, K. Kimura, T. Yagi, N. Taketoshi, T. Baba, Y. Shigesato, Thermophysical and electrical properties of Al-doped ZnO films, J. Appl. Phys. 111 (2012) 093701.